JOURNAL OF MATERIALS SCIENCE 13 (1978) 921–929

Simulation of spherical powder sintering by surface diffusion*

R. M. GERMAN†, J. F. LATHROP
Sandia Laboratories, Livermore, California 94550, USA

The surface diffusion-controlled sintering of monosized spheres is studied by a computer simulation process. The simulation is used to determine the variations in neck size and surface area as functions of both sintering time and powder packing density. Both morphology parameters are shown to be complex functions of the sintering time, contrary to numerous models. This work shows that the exponent method is not sufficient for identifying the dominant sintering mechanism.

1. Introduction

The sintering process is important to both the metallurgical and ceramic industries. Accordingly, considerable attention has been given to modelling the morphological changes accompanying sintering. The typical model experiment uses either monosized spheres or rods to study the neck growth kinetics. The analyses by Frenkel [1] and Kuczynski [2] provided the first successful theories for the initial neck growth kinetics in such model experiments. The assumptions inherent in Kuczynski's treatment limit the model to the first stage of sintering before the growing necks begin to overlap (see Fig. 1). The Kuczynski kinetic equation for neck growth is

$$(x/a)^n = C_1 t, \qquad (1)$$

where x/a is the neck radius divided by the particle radius ($x/a < 0.3$), n is the mechanism characteristic exponent, t is the isothermal time, and C_1 is a constant incorporating temperature, particle size, material properties, and geometric constants. Several analyses [1–12] have derived various forms for Equation 1. Hence it is not surprising to learn that the n value is still ambiguous for a process such as surface diffusion.

The present approach attempts to rectify the ambiguity associated with the neck growth rate for spheres that are sintering by means of a surface diffusion mechanism. The model is based on a numerical simulation of the capillarity induced morphology changes. Besides the neck growth problem, the loss in surface area is also determined for the sphere–sphere situation. Recent morphology modelling for sintering spheres [13, 14] and wires [15] has been extended to estimate the surface area reduction kinetics [16–19]. This modelling has resulted in the equation

$$\left(\frac{\Delta S}{S_0}\right)^{\gamma} = C_2 t \qquad (2)$$

where ΔS is the loss in surface area from the initial value of S_0, C_2 is a constant, and γ is a mechanism characteristic exponent that is dependent on n. Unfortunately, an uncertainty in n results in a similar uncertainty in γ.

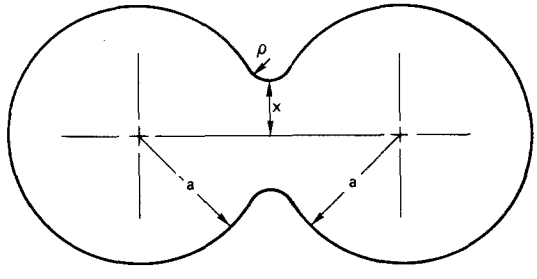

Figure 1 Model for the two sphere sintering problem.

*This work was supported by the United States Energy Research and Development Administration.
†Current address: Mott Metallurgical Corporation, Spring Lane, Farmington, CT 06032, USA.

To the experimentalist, Equation 2 is very useful because all sintering mechanisms produce a surface area reduction (unlike the case with shrinkage), and the measurements are far less tedious than neck size determinations. To establish the full value of Equation 2, it is necessary that γ be determined precisely for each mechanism. The present work is intended to serve a multiple purpose in determining both n and γ for surface diffusion-controlled sintering.

2. Background

Several different mass transport paths can initially contribute to neck growth and, in most instances, more than one path is active [20–22]. Sintering which occurs by the action of two or more mechanisms complicates the analysis of model system data [11, 21–23]. However, an even more fundamental complication is the uncertainty in the neck growth exponent n of Equation 1. In some instances (i.e., viscous flow, plastic flow, evaporation-condensation, volume diffusion adhesion, and grain boundary diffusion), the theoretical analyses are in reasonable agreement [24, 25]. One mechanism for which there is still considerable uncertainty in the assigned value of n is surface diffusion.

The theoretical analyses by Kuczynski [2] and Rockland [10] give a value of $n = 7$. Alternatively, Pines [5], Nichols and Mullins [9] and Nichols [12] derive values near 6, while Cabrera [3] and Schwed [4] suggest n values of 3 or 5 are appropriate to sintering by surface diffusion. The determinations by Nichols and Mullins [9] and Nichols [12] were based on computer simulation experiments. One reason for their value of $n = 6$ is that the simulation process gave undercutting of the sphere in the neck region. Such undercutting alters the curvature gradient from that assumed by Kuczynski and results in a lower exponent.

The specific case of surface diffusion is experimentally important. Several situations have been reported wherein surface diffusion is the predominant sintering mechanism. Indeed, it has been suggested that surface diffusion is the dominant initial stage transport mechanism for the sintering of most crystalline materials [9–13, 20]. It will be shown in the present work that the neck growth exponent for surface diffusion controlled sintering is not constant. Thus, observation of exponents ranging between 5 and 7 is not particularly representative of any one mechanism. Hence, such theoretical uncertainty hinders unambiguous interpretation of such experimental data on the basis of just the neck growth exponent.

In many instances sintering studies are approached by performing macroscopic compact shrinkage measurements. However, for the surface diffusion mechanism, densification is absent because the surface acts as both the mass source and the sink. Thus, in those instances where surface diffusion is the dominant sintering mechanism, shrinkage techniques are not applicable.

Computer simulations of various aspects of the sintering process have been reported by several authors [9, 12, 26–32]. Nichols and Mullins [9] simulated surface diffusion-controlled sintering of a line of spheres. They observed the exponent of n of Equation 1 to vary from 5.5 to 6.5 with increasing neck size. Nichols [2] similarly reported n to vary from 5.2 to 6.5 for the surface diffusion mechanism with the wire–wire geometry. At neck sizes between 0.3 and 0.6, the exponent ranges from 6.3 to 6.9. Other reports have covered the problems associated with pore rounding [31], pore migration [30], volume diffusion [27, 28], viscous flow [32] and nonisothermal shrinkage [29]. These calculations have attempted to increase the understanding of the sintering process by reconciling experimental observations to general kinetic laws.

With respect to the present problem of understanding the initial stage of surface diffusion-controlled sintering, the work of Nichols and Mullins [9] is most important. Based on the work of Mullins [33], they show that for a surface of revolution the time-dependent normal motion obeys the equation

$$\frac{\partial n}{\partial t} = (B/y)(\partial/\partial s)\,[y(\partial K/\partial s)] \qquad (3)$$

where ∂n is the outward normal motion travelled by a point on the surface in the time ∂t, y is the distance from the axis of revolution, s is the arc length along the surface, K is the surface curvature, and B is defined as follows:

$$B = D_s \sigma \delta^4 / kT \qquad (4)$$

with D_s equal to the surface self-diffusion coefficient, σ equal to the surface tension, δ equal to the interatomic distance, and kT having its usual meaning. For the initial stage of sintering, Nichols and Mullins [9] show that Equation 3 gives an

approximate neck growth law as

$$(x/a)^7 = 28Bt/a^4 \quad (5)$$

In their treatment, they generated a more exact solution to Equation 3 by a numerical finite difference approach.

One difficulty with such a simulation approach is its slow nature and hence susceptibility to cumulative error. Although volume conservation is a presumed aspect of such a solution, the results showed such not to be the case [34]. Thus, the simulation process had to be periodically interrupted to manually reinvoke volume conservation. Another problem with the Nichols and Mullins approach was that they formulated the finite difference problem in terms of arc length and tangent angle. King [27] has rejected this approach to the kinetic problem because of the cumulative errors and resulting drift in the overall sintering profiles. Indeed, our preliminary efforts with the solution techniques outlined by Nichols and Mullins met with similar difficulties. The alternative solution [27] used for the present approach is to parameterize the coordinates of a point on the surface in terms of a single variable.

3. Model

We begin by assuming that a finite set of points exist which describe the contour of a surface of revolution. The x, y coordinates of these m points are chosen such that the incremental arc lengths Δs between points are nearly equal. For the m surface points, the coordinates can be parameterized with respect to ν where ν takes on values from 1 to m. This parameterization has the advantage of handling undercutting and gives easy interpolation of x and y. We then fit $x(\nu)$ and $y(\nu)$ such that $dy/dx = 0$ at $\nu = 1$ (at the neck). This presumes zero grain boundary energy at the particle interfaces. Furthermore, for the sake of symmetry dy/dx is held constant at $\nu = m$. The symmetry point corresponds to a position on the surface at a radial angle ϕ from the sphere centre [13]. Variable powder packings can be studied by adjusting the angle ϕ. The sintering zone size as determined by ϕ is dependent on the powder packing coordination N_c as follows:

$$\phi = \cos^{-1}(1 - 2/N_c) \quad (6)$$

At any point on the arc of length s,

$$\frac{ds}{d\nu} = \left[\left(\frac{dx}{d\nu}\right)^2 + \left(\frac{dy}{d\nu}\right)^2\right]^{1/2} \quad (7)$$

The unit outward normal at any point ν is then given by

$$\left(\frac{ds}{d\nu}\right)^{-1}\left(-\frac{dy}{d\nu}\hat{x} + \frac{dx}{d\nu}\hat{y}\right) \quad (8)$$

where $\hat{x}$ and $\hat{y}$ are the unit axis vectors. At any point ν the principal radii of curvature are

$$R_1 = \frac{y(\nu)\,ds/d\nu}{dx/d\nu} \quad (9a)$$

and

$$R_2 = \frac{(ds/d\nu)^3}{(d^2y/d\nu^2)(dx/d\nu) - (d^2x/d\nu^2)(dy/d\nu)} \quad (9b)$$

The curvature $K = 1/R_1 + 1/R_2$.

The surface flux of atoms on an arbitrary surface is given as [33],

$$J_s = (B/\Omega)\nabla_s K \quad (10)$$

where $\nabla_s K$ is the surface curvature gradient and Ω is the atomic volume. For the area between two consecutive surface points, ν_1 and ν_2, the volume accumulation is given as

$$\delta A \delta n = (J_1 \delta l_1 - J_2 \delta l_2)\Omega \delta t \quad (11)$$

where δA is the surface area in the interval, and δn is the incremental outward motion of the surface. For a surface of revolution,

$$\delta l_1 = 2\pi y(\nu_1) \quad (12a)$$

and

$$\delta l_2 = 2\pi y(\nu_2) \quad (12b)$$

Combining Equations 10 to 12, the normal motion with respect to time can then as expressed as

$$\frac{\delta n}{\delta t} = \frac{2\pi B}{\delta A}\left[y(\nu_2)\nabla_s K(\nu_2) - y(\nu_1)\nabla_s K(\nu_1)\right] \quad (13)$$

and

$$\delta A = 2\pi \int_{\nu_1}^{\nu_2} y(ds/d\nu)\,d\nu \quad (14)$$

Therefore, by representing $y(\nu_2)$ as y_2, etc., the normal motion is given approximately by

$$\frac{\partial n}{\partial t} = \frac{B(y_2\nabla_s K_2 - y_1\nabla_s K_1)}{\int_{\nu_1}^{\nu_2} y(ds/d\nu)\,d\nu} \quad (15)$$

It should be noted that in the limit as ν_1 and ν_2 approach each other Equation 15 is the same as

Equation 3. The solution to Equation 15 was achieved by a means of a numerical approach wherein for an arbitrary point on the surface designated i, the curvatures are given as

$$\nabla_s K_{i-1/2} \approx \frac{K_i - K_{i-1}}{[(y_i - y_{i-1})^2 + (x_i - x_{i-1})^2]^{1/2}} \quad (16a)$$

and

$$\nabla_s K_{i+1/2} \approx \frac{K_{i+1} - K_i}{[(y_{i+1} - y_i)^2 + (x_{i+1} - x_i)^2]^{1/2}} \quad (16b)$$

Finally, the surface area between half intervals is given as

$$\int_{i-1/2}^{i+1/2} y(\mathrm{d}s/\mathrm{d}\nu)\,\mathrm{d}\nu \approx$$

$$\tfrac{1}{2}[y_{i+1/2}\,\mathrm{d}s/\mathrm{d}\nu|_{i+1/2} + y_{i-1/2}\,\mathrm{d}s/\mathrm{d}\nu|_{i-1/2}] \quad (17)$$

Thus, the normal motion $\partial n/\partial t$ for the point i can be reasonably approximated as

$$\left.\frac{\delta n}{\delta t}\right|_i \approx \frac{B(y_{i+1/2}\nabla_s K_{i+1/2} - y_{i-1/2}\nabla_s K_{i-1/2})}{\int_{i-1/2}^{i+1/2} y(\mathrm{d}s/\mathrm{d}\nu)\,\mathrm{d}\nu} \quad (18)$$

By imposing symmetry arguments at $\nu = 1$ and $\nu = m$, it can be shown that

$$\left.\frac{\delta n}{\delta t}\right|_1 = \frac{By_{1+1/2}\nabla_s K_{1+1/2}}{\int_1^{1+1/2} y(\mathrm{d}s/\mathrm{d}\nu)\mathrm{d}\nu} \quad (19a)$$

$$\left.\frac{\delta n}{\delta t}\right|_m = -\frac{By_{m-1/2}\nabla_s K_{m-1/2}}{\int_{m-1/2}^{m} y(\mathrm{d}s/\mathrm{d}\nu)\mathrm{d}\nu} \quad (19b)$$

For the present simulations, the initial interparticle neck size was preset at 0.01 [9, 12]. After finding $\delta n/\delta t$ for every point on the surface, it is then necessary to select the appropriate time interval. The time interval was calculated such that

$$\Delta t = \frac{\alpha \Delta s}{\underset{i}{\mathrm{Max}}\,(\delta n/\delta t|_i)} \quad (20)$$

where $\alpha < 1$ is a parameter selected to ensure stability. The determination of Δt then allows the surface to be shifted, where the change in surface is given by

$$\frac{\mathrm{d}x_i}{\mathrm{d}t} = \left(\left.\frac{\partial n}{\partial t}\right|_i\right)\left(-\frac{\partial y}{\partial s}\Big/\frac{\partial s}{\partial \nu}\right) \quad (21a)$$

$$\frac{\mathrm{d}y_i}{\mathrm{d}t} = \left(\left.\frac{\partial n}{\partial t}\right|_i\right)\left(\frac{\partial x}{\partial s}\Big/\frac{\partial s}{\partial \nu}\right) \quad (21b)$$

To calculate the new surface coordinate we use a low-order Runge–Kutta formulation

$$\tilde{x}_i = x_i - \Delta t \frac{\partial n}{\partial t} \cdot \left(\frac{\partial y}{\partial s}\Big/\frac{\partial s}{\partial \nu}\right) \quad (22a)$$

$$\tilde{y}_i = y_i + \Delta t \frac{\partial n}{\partial t} \cdot \left(\frac{\partial x}{\partial s}\Big/\frac{\partial s}{\partial \nu}\right) \quad (22b)$$

Using these approximate values $\tilde{x}_i, \tilde{y}_i$ at the next time, we recalculate

$$\frac{\partial \tilde{n}_i}{\partial t}, \quad \frac{\partial \tilde{y}_i}{\partial s}, \quad \frac{\partial \tilde{x}_i}{\partial s}$$

The new surface coordinates are then given by

$$x_i^{\mathrm{new}} = \frac{1}{2}\left[x_i + \tilde{x}_i - \Delta t \frac{\partial \tilde{n}}{\partial t}\left(\frac{\partial \tilde{y}}{\partial s}\Big/\frac{\partial s}{\partial \nu}\right)\right] \quad (23a)$$

$$y_i^{\mathrm{new}} = \frac{1}{2}\left[y_i + \tilde{y}_i - \Delta t \frac{\partial \tilde{n}}{\partial t}\left(\frac{\partial \tilde{x}}{\partial s}\Big/\frac{\partial s}{\partial \nu}\right)\right] \quad (23b)$$

This approach allows a larger time step and smooths out the oscillations that occur when using the simple Euler procedure of

$$x_i^{\mathrm{new}} = x_i + \Delta t \cdot \left.\frac{\mathrm{d}x}{\mathrm{d}t}\right|_i.$$

After moving the surface to the new coordinates, a polynomial fit is performed. This surface contour is integrated to find the s_i values which are, in turn, used to interpolate the new coordinates such that Δs is approximately constant, thereby maintaining the simulation accuracy. Also several simulations were conducted with various arc spacings to determine the appropriate spacing which minimizes both the error and computational time.

Convergence of this approach was tested by perturbing a sphere and observing its return to sphericity. The accuracy of the simulation was continually monitored by integrating the volume of revolution. Volume conservation was used to detect the onset of significant cumulative errors. All simulations were terminated when the volume loss or gain exceeded 1% of the original value. Stability in the simulation is partially governed by the value assigned to α in Equation 20. Several simulations were conducted with a range of α values to determine the maximum acceptable value of α. For these studies, a value of 0.8 proved to be acceptable. Furthermore, a test for stability

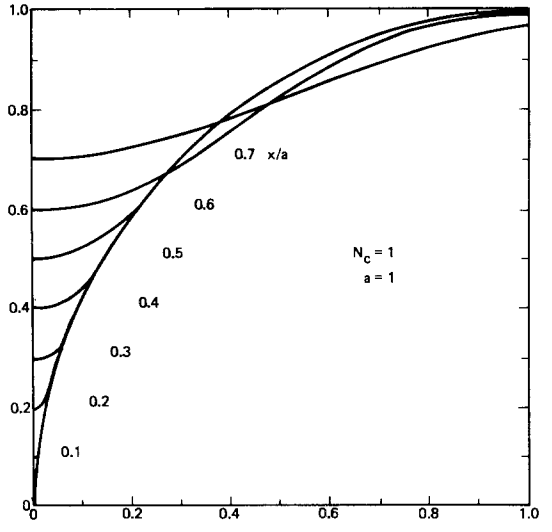

Figure 2 Neck profiles for two spheres sintering by a surface diffusion.

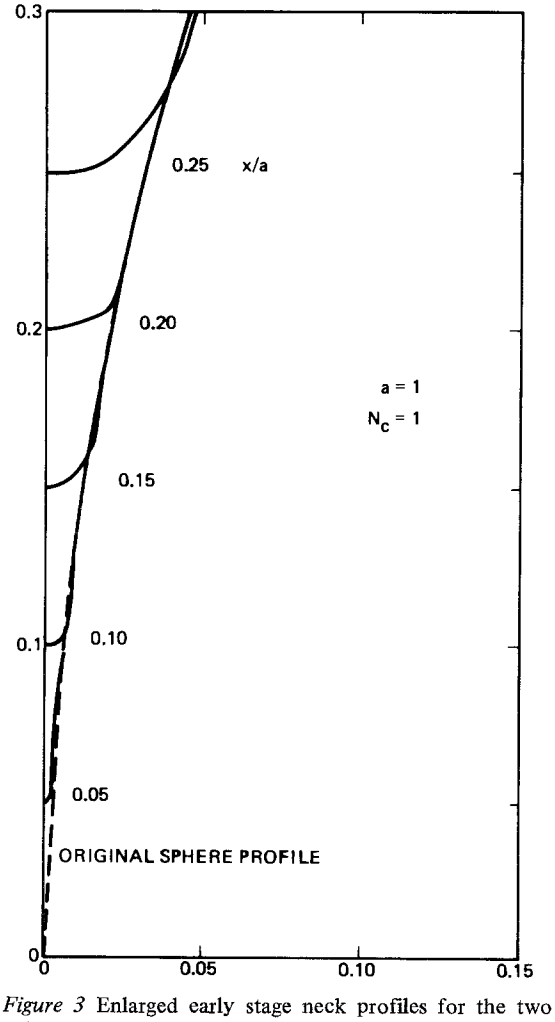

Figure 3 Enlarged early stage neck profiles for the two sphere simulation showing the sphere undercutting in the neck region.

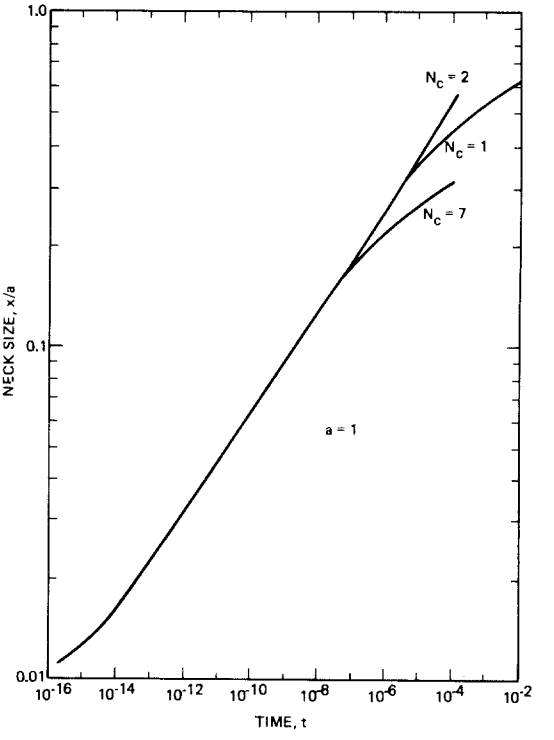

Figure 4 Neck growth time dependence for $N_c = 1$, 2, and 7.

was possible through the curvature. It was observed that comparison of the point-to-point curvatures gave early indications of instability due to cumulative errors. Fortunately, these errors occurred after appreciable neck growth, well beyond the initial stage of sintering where previous neck growth models have been applied.

4. Results

The computations were carried out on a CDC 6600 digital computer for interparticle coordinations N_c of 1, 2, and 7. The interparticle coordination of 1 represents two isolated spheres sintering together, while $N_c = 2$ corresponds to a line of spheres. The coordination of 7 is typical of a loose-packed bed of spheres during the initial stage sintering [35, 36]. The coordination number is linked to the surface zone size contributing to initial neck growth by assuming $1/N_c$ of the sphere contributes to each neck. For this analysis it is assumed that such isosintering zones can be represented by a spherical cone as described by Equation 6 [13].

The ability to monitor continuously the volume provides a means of detecting cumulative computational errors. In all cases, the loss of volume

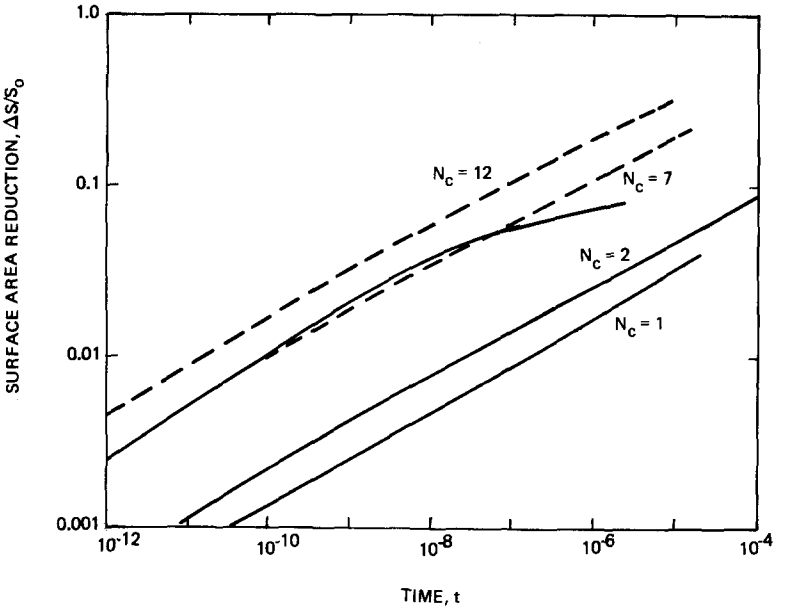

Figure 5 Kinetics for the surface area reduction for spheres sintering by surface diffusion; packing coordinations of 1, 2, and 7 (dashed lines are estimated from $N_c = 1$ behaviour).

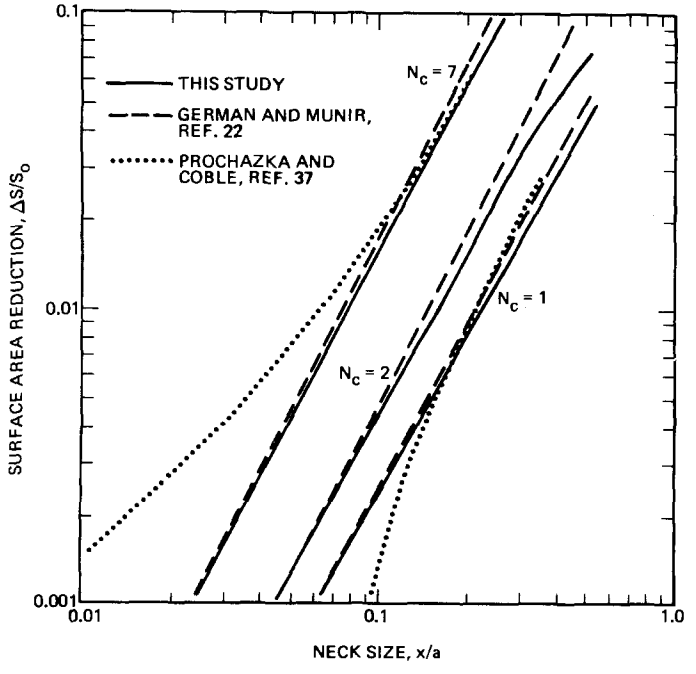

Figure 6 Relation between the specific surface area reduction $\Delta S/S_0$ and the neck size for sphere–sphere sintering by surface diffusion at packing coordinations of 1, 2, and 7.

conservation occurred after appreciable neck growth. The neck profiles for $N_c = 1$ for x/a up to 0.7 are shown in Figs. 2 and 3. These simulations were all performed with both "B" and "a" set at unity. Undercutting of the sphere is apparent in these profiles. Qualitatively, it appears that the undercutting in the present simulation is less than that observed previously [9].

The time dependence of the neck growth for the three coordinations is shown in Fig. 4. The time units for the abscissa are effectively normalized with respect to the particle size and material constants by setting $B = 1$ and $a = 1$. The initial behaviour for all three packing coordinations are similar. Such similarity results from the essentially localized nature of the initial neck growth.

During the incipient sintering ($x/a \leqslant 0.1$), mass transport originates from the immediate region on the sphere around the neck. Thus, as shown by Fig. 4, the packing coordination is of little influence on the neck growth rate. At extended time,

the packing coordination influences the curvature gradient and thereby alters the neck growth kinetics.

In a similar manner, the surface area reduction ($\Delta S/S_0$) kinetics are shown in Fig. 5. The dashed lines in Fig. 5 for $N_c = 7$ and 12 are calculated from the $N_c = 1$ data assuming that $\Delta S/S_0$ is proportional to N_c. In the $N_c = 7$ case, the agreement between the two curves indicates that the early neck growth process occurs essentially independently of powder packing. At the point where neighbouring neck effects begin to become significant, a deviation in the simulation result can be observed. The relation between surface area reduction and neck growth is shown in Fig. 6 on a log–log basis. For comparison, the predictions of the surface-transport morphology model [16] are included in Fig. 6. Also, the results of Prochazka and Coble's [37] integration of Nichols and Mullins results are shown in Fig. 6. The reduced degree of surface area loss with neck growth as determined by simulation is due to undercutting. Undercutting reduced the local curvature gradient at the expense of an increased surface area. The predicted slopes for log ($\Delta S/S_0$) versus log (x/a) at $x/a = 0.2$ are 1.80, 1.84, and 2.02 for $N_c = 1$, 2, and 7 respectively [16]. For comparison, the observed slopes in this study at $x/a = 0.2$ are 1.84, 1.85, and 1.91 respectively.

Based on the kinetic behaviours shown in Figs. 4 and 5, the slopes have been extracted for a fit to Equations 1 and 2. The resulting exponents, n and γ, are shown as functions of x/a and N_c in Fig. 7. The results reported by Nichols and Mullins [9] have been included in Fig. 7 for comparison.

The predicted mean γ values for $N_c = 1, 2$, and 7 are 3.89, 3.80, and 3.47 respectively, using $n = 7$ [16]. The varying n and γ values for the present results represent the effects of undercutting and changing geometries [27]. The lower n values observed in the previous simulation study [9] are most probably due to the larger degree of initial sphere undercutting resulting from the different numerical approach. An important point in this study is that the n values increase above 7 with $x/a > 0.25$ for all coordinations. Furthermore, both studies show the n values are not constant for initial stage sintering of spheres by surface diffusion. However, the present approach suggests n values of ~ 7 are representative of the initial stage.

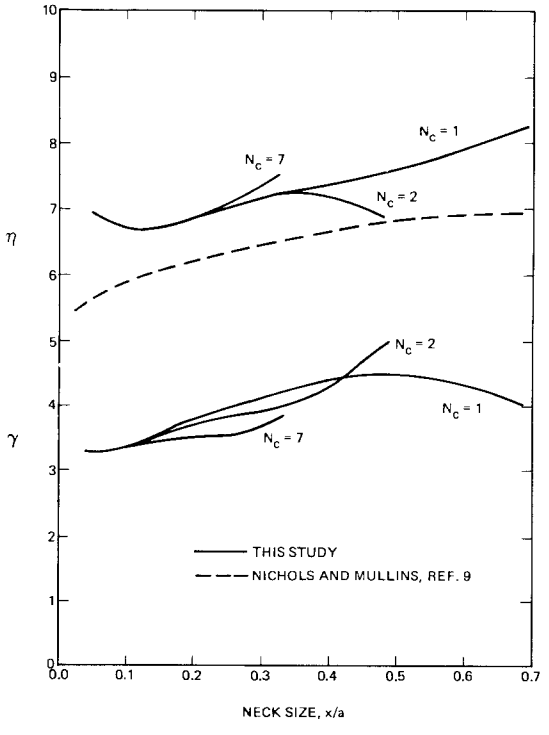

Figure 7 Dependence of n from Equation 1 and γ from Equation 2 on the neck size powder coordination.

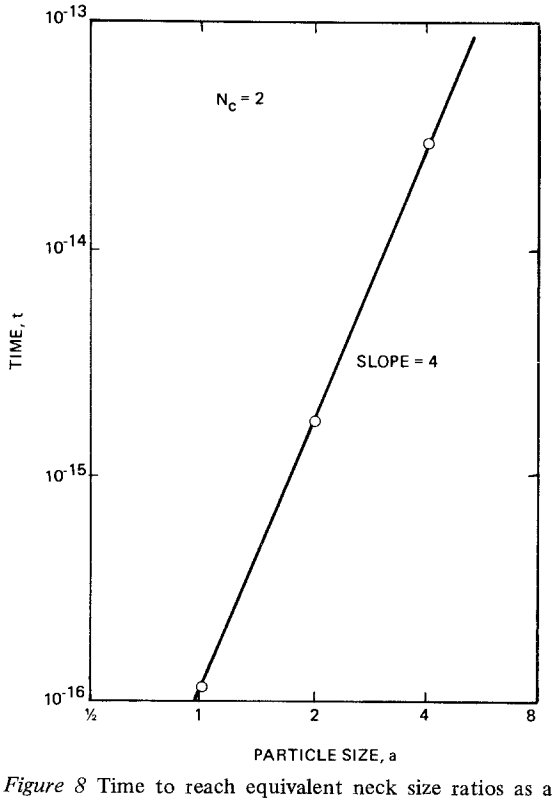

Figure 8 Time to reach equivalent neck size ratios as a function of particle size, illustrating agreement with the a^4 dependence predicted by the Herring [38] scaling laws.

Three additional simulations were conducted to test for the particle size dependence. The Herring scaling law predicts a particle size dependence of a^4 for sintering controlled by surface diffusion [38]. This prediction is in agreement with the neck growth kinetic laws due to Kuczynski [2] and others [9, 10]. The times to reach various neck size ratios were determined for $a = 1, 2$, and 4. The resulting particle size dependence was determined to be a^4, as illustrated in Fig. 8.

5. Discussion

The present numerical simulation results apply to the initial stage of sintering of monosized spheres. This sintering process is controlled by surface diffusion and occurs without densification. For a surface diffusion process, the present simulations give a best approximation to the neck growth behaviour as

$$(x/a)^7 = 80Bt/a^4 \quad (24)$$

for the sphere–sphere problem. However, such an equation is an imprecise simplification of the behaviour during initial stage sintering. A similar approximation for the specific surface area reduction rate can be expressed as

$$(\Delta S/S_0)^{3.5} = 1100Bt/a^4 \quad (25)$$

for $N_c = 7$. Equations 24 and 25 are approximations, since as Fig. 7 shows, n and γ are not constant. The dependence of n on x/a is not new; King [27] showed that a rigorous solution to Kuczynski's original model gave a varying n for both surface and volume diffusion. Thus, the comparison of experimental data to the mathematical format of either Equations 1 or 2 must be performed with care. Traditionally, the identification of the dominant sintering mechanism is based on agreement with theoretically predicted n values. The simulation results for surface and volume diffusion suggest that a spectrum of n values can be expected in such experiments [9, 12, 27]. Furthermore, the experimental possibility of multiple diffusion paths creates an even greater range of process exponents, generally resulting in lower n and γ values than those applicable to a surface diffusion-controlled process.

The differences in neck growth exponents between Equation 24 and Nichols and Mullins [9] is due to the undercutting differences. The degree of undercutting is sensitive to the numerical approach used in solving Equation 3. Undercutting has been subdued in the present results by the particular numerical solution adopted for Equation 3. The present approach gives better agreement with the modified catenoid model [19]. This model represents the minimum surface energy configuration for a given neck size which still maintains the chemical potential gradients. The appearance of undercutting suggests that the curvature gradient and surface free energy are both concurrently acting on the sintering morphology during initial stage sintering [25]. The effect of undercutting on the surface area reduction rate is small.

It is important to realize that the degree of undercutting and the neck growth rate exponent are interrelated. Both, in turn, are dependent on the finite difference formulation used in solving the surface diffusion sintering problem.

The present simulation approach has the advantages of providing an interlinking of neck growth and surface area reduction while testing for accuracy through volume conservation. However, the approach is generally limited to the initial stage of sintering in which large curvature gradients are present.

6. Conclusions

For the case of the surface diffusion mechanism, the theoretical models for the neck growth rate during the initial stage of sintering are in disagreement. Computer simulation results suggest a varying neck growth exponent. However, during the initial sintering stage a value between 6 and 7 can be expected for the neck growth kinetics. The differing simulation results represent the lower degree of undercutting due to the numerical solution techniques employed by the present authors.

References

1. J. FRENKEL, *J. Phys. (USSR)* **9** (1945) 385.
2. G. C. KUCZYNSKI, *Trans. AIME* **185** (1949) 169.
3. N. CABRERA, *ibid* **188** (1950) 667.
4. P. SCHWED, *ibid* **191** (1951) 191.
5. B. YA. PINES, *Usp. Fiz. Nauk. (USSR)* **52** (1954) 501.
6. W. D. KINGERY and M. BERG, *J. Appl. Phys.* **26** (1955) 1205.
7. R. L. COBLE, *J. Amer. Ceram. Soc.* **41** (1958) 55.
8. D. L. JOHNSON and I. B. CUTLER, *ibid* **46** (1963) 541.
9. F. A. NICHOLS and W. W. MULLINS, *J. Appl. Phys.* **36** (1965) 1826.
10. J. G. R. ROCKLAND, *Acta Met.* **14** (1966) 1273.

11. *Idem, ibid* **15** (1967) 277.
12. F. A. NICHOLS, *ibid* **16** (1968) 103.
13. R. M. GERMAN and Z. A. MUNIR *Met. Trans. B* **6B** (1975) 289.
14. *Idem, Met. Trans. A* **6A** (1975) 2229.
15. *Idem, J. Mater. Sci.* **10** (1975) 1719.
16. *Idem,* "Materials Science Research" Vol. 10, edited by G. C. Kuczynski (Plenum Press, New York, 1975) p. 249.
17. *Idem, ibid* p. 259.
18. R. M. GERMAN and Z. A. MUNIR, *J. Mater. Sci.* **11** (1976) 71.
19. *Idem, J. Amer. Ceram. Soc.* **59** (1976) 379.
20. T. L. WILSON and P. G. SHEWMON, *Trans. TMS-AIME* **236** (1966) 48.
21. D. L. JOHNSON, *J. Appl. Phys.* **40** (1969) 192.
22. M. F. ASHBY, *Acta Met.* **22** (1974) 275.
23. R. M. GERMAN and Z. A. MUNIR, *Int. J. Powder Tech.* **12** (1976) 37.
24. F. THUMMLER and W. THOMMA, *Metall. Rev.* **12** (1967) 69.
25. G. C. KUCZYNSKI, *Advan. Colloid Interface Sci.* **3** (1972) 275.
26. F. A. NICHOLS, *J. Appl. Phys.* **37** (1966) 2805.
27. R. T. KING, "Numerical Methods for Sintering by Volume Diffusion," Oak Ridge National Laboratory, Oak Ridge, Tennessee, Report ORNL-TM-2014, 1968.
28. K. E. EASTERLING and A. R. THOLEN, *Z. Metallkde.* **61** (1970) 928.
29. T. Z. FAHIDY and J. R. WYNNYCKYJ, *Simulation* **30** (1973) 73.
30. A. J. MARKWORTH and W. OLDFIELD, "Materials Science Research," Vol. 6, edited by G. C. Kuczynski (Plenum Press, New York, 1973) p. 209.
31. K. BREITKREUTZ and D. AMTHOR, *Metall.* **29** (1975) 990.
32. G. J. COSGROVE, J. A. STROZIER JR. and L. L. SEIGLE, *J. Appl. Phys.* **47** (1976) 1258.
33. W. W. MULLINS, *J. Appl. Phys.* **28** (1957) 333.
34. F. A. NICHOLS, Private communication.
35. F. N. RHINES, R. T. DEHOFF and J. KRONSBEIN, "A Topological Study of the Sintering Process," University of Florida, Gainsville, Florida, Final Report US AEC Contract N. AT-(40-1)-2581, 1969.
36. R. L. EADIE, D. S. WILKINSON and G. C. WEATHERBY, *Acta Met.* **22** (1974) 1185.
37. S. PROCHAZKA and R. L. COBLE, *Phys. Sintering* **2** (1970) 1.
38. C. HERRING, *J. Appl. Phys.* **21** (1950) 301.

Received 10 June and accepted 15 September 1977.